Research Article

Tauqir Nasir, Omer Kalaf, Mohammed Asmael, Qasim Zeeshan, Babak Safaei*, Ghulam Hussain, and Amir Motallebzadeh

The experimental study of CFRP interlayer of dissimilar joint AA7075-T651/Ti-6Al-4V alloys by friction stir spot welding on mechanical and microstructural properties

https://doi.org/10.1515/ntrev-2021-0032
received May 9, 2021; accepted May 17, 2021

Abstract: The present study focused on two dissimilar metal alloys: AA7075-T651 and Ti-6Al-4V alloys with additional carbon fiber-reinforced polymer (CFRP) as an interlayer were welded together by friction stir spot welding (FSSW). The effect of welding parameters (rotational speed and dwell time) and carbon fiber-reinforced polymer on mechanical and microstructural properties of a weld joint was investigated. The obtained results explore the parametric effects on mechanical properties of the weld joint. The maximum tensile shear load 2597.8 N was achieved at the rotational speed of 2,000 rpm and dwell time of 10 s. While at the same rotational speed, 54.7% reduction in the tensile shear load was attained at shorter dwell time of 5 s. Therefore, dwell time plays an important role in the tensile shear load of a weld joint. The scanning electron microscope (SEM-EDS) results show the formation of intermetallic compound of Ti_3Al and Ti-Al-C that significantly affect the mechanical and microstructural properties of the weld joint. Moreover, the effect of the rotational speed on micro-hardness was found at significant than dwell time. The microhardness of the weld joint increase by 18.90% in the keyhole rather than the stir zone and the thermomechanical affected zone, which might be due to the presence of ternary (Ti-Al-C) intermetallic compound.

Keywords: friction stir spot welding, titanium alloys, aluminum alloys, interlayer, carbon fiber-reinforced polymer, welding parameters

1 Introduction

The demand of lightweight alloys in automotive and aerospace industries increases because of global resources and environment problems tending to be more and more serious; therefore more attention is paid on weight reduction. The use of lightweight alloys reduces the carbon emission and improves the fuel efficiency [1]. In automotive sector, the main aim for future years is to reduce the fuel consumption and consequently the harmful gas emission [2]. The 10% reduction in vehicle weight leads to reduce 5.5% of fuel consumption, *i.e.*, one-pound reduction in vehicle weight can reduce 20-pound carbon dioxide over a life period of a vehicle [3]. Therefore, the requirement of lightweight alloys like aluminum, magnesium, titanium, and aluminum matrix composite increased instead of only steel alloys to reduce the weight [4]. Weight reduction is a critical challenge in automotive and aerospace industries to improve performance [5]. Nowadays, composites are playing a vital role in the modern society to fulfil the increasing demand of structural materials [6]. Carbon fiber belongs to the category of carbon material, which are considered very important reinforcement in advanced composite [7] due to their mechanical properties [8]. Carbon fiber-reinforced polymer (CFRP) is an ideal material for the designing and construction of hybrid structure of metal and composite [9]. Carbon fiber/aluminum composite have better strength and wear

* **Corresponding author: Babak Safaei,** Department of Mechanical Engineering, Eastern Mediterranean University, Famagusta, North Cyprus via Mersin 10, Turkey; Department of Mechanical Engineering Science, University of Johannesburg, Gauteng 2006, South Africa, e-mail: babak.safaei@emu.edu.tr
Tauqir Nasir, Omer Kalaf, Mohammed Asmael, Qasim Zeeshan: Department of Mechanical Engineering, Eastern Mediterranean University, Famagusta, North Cyprus via Mersin 10, Turkey
Ghulam Hussain: Faculty of Mechanical Engineering, GIK Institute of Engineering Sciences & Technology, Topi, 23460, Pakistan
Amir Motallebzadeh: Koç University Surface Science and Technology Center (KUYTAM), Sariyer, Istanbul, Turkey

resistance in contrast of unreinforced aluminum matrix [10]. Carbon-based material can be added into nanocomposite to improve thermal conductivity [11], whereas carbon nanotubes are suitable for electrical and thermal application [12]. Porous composite material are widely used in energy absorbing system, sound absorber, heat exchanger, and construction materials due to its damage tolerance [13]. Recently, composite materials have prompt the worldwide investigation to manufacture advanced structure with superior mechanical properties [14]. CFRP composite exhibits excellent mechanical characteristics in terms of high level of stiffness-to-weight ratio and strength-to-weight ratio [15]. Consequently, CFRP composite are widely admire in many manufacturing sector application, such as aerospace, medical services, aeronautics, and automotive industries [16]. Conversely, laminated composite material has some issues such as matrix cracking, interlayer stress component, and interfacial debonding [17]. Therefore, only carbon composite material can be used to design a lightweight structure, which shows high performance in engineering applications [18]. However, carbon fiber reinforced are being used in concrete where it shows better fracture toughness and the enhanced compressive strength of the concrete [19]. At the elevated temperature, composite lacked the damage tolerance and it paved the way to nanocomposite [20]. The lack of ductility is a greatest concern in CFRP materials when used as prestressing reinforcements [21]. Application of CFRP in transportation industry, where energy efficiency is required, are rapidly growing due to inherent capacity to reduce the weight of an aircraft or car. It has outstanding corrosion resistance, environmental stability, and high fatigue performance which make it attractive for many industries [22]. Filament-wounded CFRP is the most effective solution for the high-pressure storage vessel [23]. Conversely, lightweight alloys like aluminum and titanium alloys play a vital role in automobile and aerospace industries: aluminum alloys reduce the weight and cost and titanium alloys enhance the strength, corrosion resistance, and high temperature workability [24].To use these materials for structure construction, a welding procedure is required. However, welding of these materials by conventional fusion welding is not possible because of high welding temperature [25]. In automotive industry, spot welding is a most well-known process, although welding of light alloys faces metallurgical problems [26]. A few decades ago, resistance spot welding (RSW) was the primary method of spot welding of aluminum sheet despite the excessive porosity and surface indentation, which severely affects the strength and fatigue performance of the weld joint. Higher electric power energy is required for the RSW of aluminum alloys, which restricts its extensive applications [27]. However, the joining of aluminum and titanium is a challenging process because of a huge difference in chemical, physical, and metallurgical properties [24].

Friction stir spot welding (FSSW) is a variant of linear friction stir welding (FSW) developed and carried out in the automotive industry as a substitute of resistance spot welding (RSW). FSW is a novel welding process invented and patented by TWI in 1991 [28]. Friction stir welding of aluminum alloys retains good mechanical and metallurgical properties [29]. Mazda Motor Corporation was the first company to report the use of FSSW in automotive assembly line in the production of rear door and bonnet of Mazda RX-8 in 2003 [30]. FSSW process has the capacity to eradicate the traditional fusion welding problems of low-density alloys like copper, aluminum, magnesium, titanium, and even metal matrix composites [31]. Some other solid-state joining processes were developed to joint dissimilar alloys, such as ultrasonic welding [32], laser welding [33], friction welding (FW) [34], FSW [35], friction stir interlocking [36], and FSSW [37]. In these methods, the joining proceeds at the solid state instead of the liquid state, and the formation of intermetallic compound (IMC) expected to be reduced because of slow diffusion. In friction stir welding of dissimilar aluminum and titanium alloys, different types of IMC formation were detected, namely, $TiAl_3$, TiAl, and Ti_3Al in AA6061/Ti-6Al-4V joint [34] and AA2024/Ti-6Al-4V alloy joint [38]. Plaine *et al.* [39] apply the friction stir spot weld on AA5754 and Ti-6Al-4V alloys and study the influence of dwell time on the microstructure of the interface and lap shear strength of the welded joint. On the interface, mainly $TiAl_3$ (IMC) layers were found. Dwell time has a significant influence on the diffusion process of FSSW, and it affects the mechanical properties of the joints. The optimizing thickness of the $TiAl_3$ layer is a key issue to obtain high-strength Ti/Al dissimilar weld joints. High dwell time resulted in an excessive increase of IMC thickness, which decreases the mechanical properties of the weld joint. Chen and Nakata [40] welded dissimilar ADC12 alloy and pure Ti by the friction stir welding technology. The maximum failure load of the lap joint reached 62% that of ADC12 Al alloy base metal. $TiAl_3$ intermetallic phase is formed at the weld interface due to the Al-Ti diffusion reaction, which strongly depends on the welding speed of the process and thus affects the mechanical properties of the joints. Choi *et al.* [41] studied the relationship between the microstructure of Ti and Al and IMC layers generated at the weld interface, mechanical properties, and fracture behavior of pure Ti and Al joint welded by FSSW. This finding shows that the increase of the probe offset and the rotational speed increased the thickness of the IMC layers. The formation of the IMC layer is $TiAl_3$,

TiAl, and Ti_3Al. The $TiAl_3$ compound layer is formed at the lowest free energy, and the formation of TiAl and Ti_3Al is attributed to the Al diffusion from the $TiAl_3$ layer. Cheepu *et al.* [42] applied aluminum in FW of steel to titanium as an interlayer and investigated the mechanical properties of the weld joint. The obtained friction weld joint with aluminum inserts between steel and titanium alloy prevents the formation of IMC in the weld interface. The tensile strength of the aluminum inserted weld joint is higher than the direct weld joint.

Cao *et al.* [43] fabricate a carbon fiber-reinforced AA5052 bulk composite by multiple-pass friction stir processing (FSP) to improve the wear resistance of AA5052 and investigated the mechanical, microstructural, and tribological performance of the composite. The result showed 46.8% increase in the hardness of the composite compared to base metal and showed 18.6% higher tensile strength and 13.0% higher elongation in a composite fabricated at 1,000 rpm and 75 mm/min of welding speed. Goushegir *et al.* [44] reported the feasibility of friction spot joining of AA2024-T3/CF-PPS to investigate the microstructure of the joint and the process temperature. The maximum lap shear strength up to 31 and 43 MPa was achieved in bare and alclad specimens, respectively. Esteves *et al.* [45] applied Taguchi and analysis of variance to investigate the effect of process parameters (rotational speed, joining time, plunge depth, and joining force) on the microstructure and mechanical strength of AA6181-T4/CF-PPS double lap shear joints by friction spot joining. The joint showed good mechanical strength, which vary from 2,107 to 3,523 N. The obtained results indicated that the parameters that have more influence on the lap shear strength were rotational speed (34.77%) followed by joining time (32.37%), plunge depth (20.70%), and joining force (12.15%). Ageorges and Ye [46] applied the resistance welding between Al7075-T6 and carbon fiber (CF)-reinforced polyetherimide (PEI) to investigate the strength of a lap shear joints. The obtained results show that the lap shear strength of AA7075-T6/CF-PEI joint were larger than 20 MPa. SEM and atomic force measurement (AFM) revealed that the low welding time resulted in the low lap shear strength and induced incomplete filling of micro-porosity on the aluminum alloy or no bounding, and that the high welding time led to highest lap shear strength and also causes the thermal degradation in this process. Applications of interlayer help to enhance the mechanical properties and prevent the formation of the intermetallic compound during the FSSW process. Interlayer will produce diffusion barrier between the two plates and will deform during welding [42]. The CFRP is used as an interlayer due to its low thermal conductivity than aluminum; therefore, it can act as an obstacle between two plates and can absorb the temperature [47]. Madhusudhan Reddy and Venkata Ramana [48] studied the role of nickel as an interlayer to improve the properties of maraging steel and low alloy steel by FW. The obtained results reveals improvement in hardness, tensile strength, and impact toughness. Shojaei Zoeram and Akbari Mousavi [49] investigated the effect of copper interlayer thickness in dissimilar welding of nitinol shape memory alloy to Ti-6Al-4V by YAG laser beam and observed the effects on microstructure, chemical composition, mechanical properties, and fracture behavior. The results show that the thickness of 75 μm tensile strength and elongation of the joint increased and more increment in thickness resulted in deterioration in mechanical properties. Xu *et al.* [50] fabricated the joint of Mg-Al-Zn alloy sheet by FSSW with and without Zn interlayer and investigated the influence on microstructure and mechanical properties of the weld joint. The addition of the Zn interlayer weld joint shows a significant improvement in the tensile strength from 2.4 to 4 kN. Kalaf *et al.* [51] applied CFRP as an interlayer in similar aluminum alloy AA5052 to investigate the effect of the welding parameter (rotational speed and dwell time) on the mechanical properties, joint efficiency, and microstructure of the friction stir spot weld joint. The obtained result reveals that the joint efficiency increased by 39.5% at higher rotational and lower dwell time compared to the lower rotational speed. A significant improvement in hardness (29%) was founded in the key whole at high rotational speed and high dwell time.

In this present study, the aluminum alloy 7075-T651 and titanium alloy Ti-6Al-4V, which are widely used in industries, were welded with the CFRP interlayer as the lap-welded joint by FSSW. The effect of CFRP interlayer and welding parameters on mechanical and microstructural properties weld joint has been investigated. The main objective of this study is to evaluate the effect of CFRP welding parameters (rotational speed and dwell time) and CFRP interlayer on the performance of mechanical properties (tensile shear load and hardness) and microstructural properties (SEM-EDS) of the weld joints. The figure shows the graphical abstract of the process.

2 Experimental procedure

This study is on AA7075-T651, and Ti-6Al-4V alloy plates with 0.5 mm thickness of CFRP as an interlayer were welded by FSSW. This process is shown in Figure 1. The samples were selected according to the JIS Z3136 standard [52] with sample dimensions of 100 × 35 × 4 mm (Figure 2a). All experiments were conducted on semi-automatic milling machine (VERNIER-S.A. 06340-LA

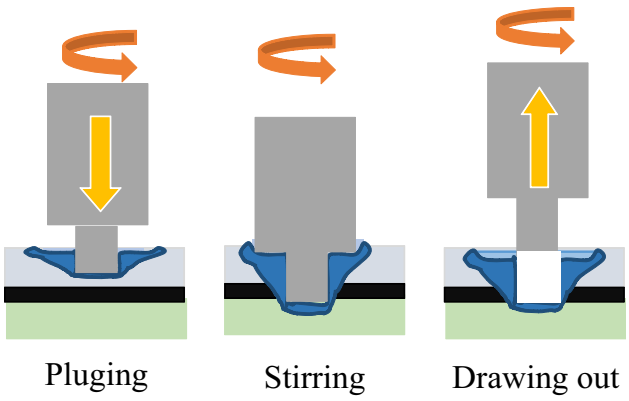

Figure 1: Illustration of FSSW process.

TRINITE) model type FV250E. To protect the metal from contaminants that can produce oxides, both faying surfaces of the plates were cleaned with alcohol. Aluminum AA7075-T651 alloy plate was placed at the top because of its low melting temperature which helps in easy penetration compared to titanium Ti-6Al-4V alloy plate. The overlap between the two plates are 35 × 35 mm with the CFRP interlayer. The joint is made at the center of the overlap points, which are marked by cross sign in Figure 2c. The high-strength H-13 steel tools were used with the shoulder diameter of 16 and 5 mm of cylindrical pin diameter and 5.8 mm long pin length (Figure 2a). A special assembly of two steel plates was created with

Table 1: Two-level 2^k full factorial design of experiment

Sample no.	Stdorder	Runorder	A	B	Rotational speed	Dwell time (s)
1	6	1	1	1	2,000	10
2	3	2	0	−1	1,400	5
3	1	3	−1	−1	1,000	5
4	2	4	−1	1	1,000	10
5	4	5	0	1	1,400	10
6	5	6	1	−1	2,000	5

guided rail that has 35 mm width and 2 mm depth at the middle of the upper and lower steel plates. Aluminum and titanium alloys with the CFRP interlayer were laid down in this assembly and then screwed tightly to keep the both plates stick together to avoid any misalignment in specimens during the welding process (Figure 2b). Full factorial design of experiment was conducted with two quantitative levels (rotational speed with three level and dwell time with two level) as welding parameters. These welding parameters were fully randomized by using Minitab 18.1 software (Table 1). The temperature evaluation of the top AA7075-T651 alloy plate was monitored by using (Thermometer PCE-T390) during the FSSW process. The maximum temperature obtained during the process considered a peak temperature on the top surface of metal plate.

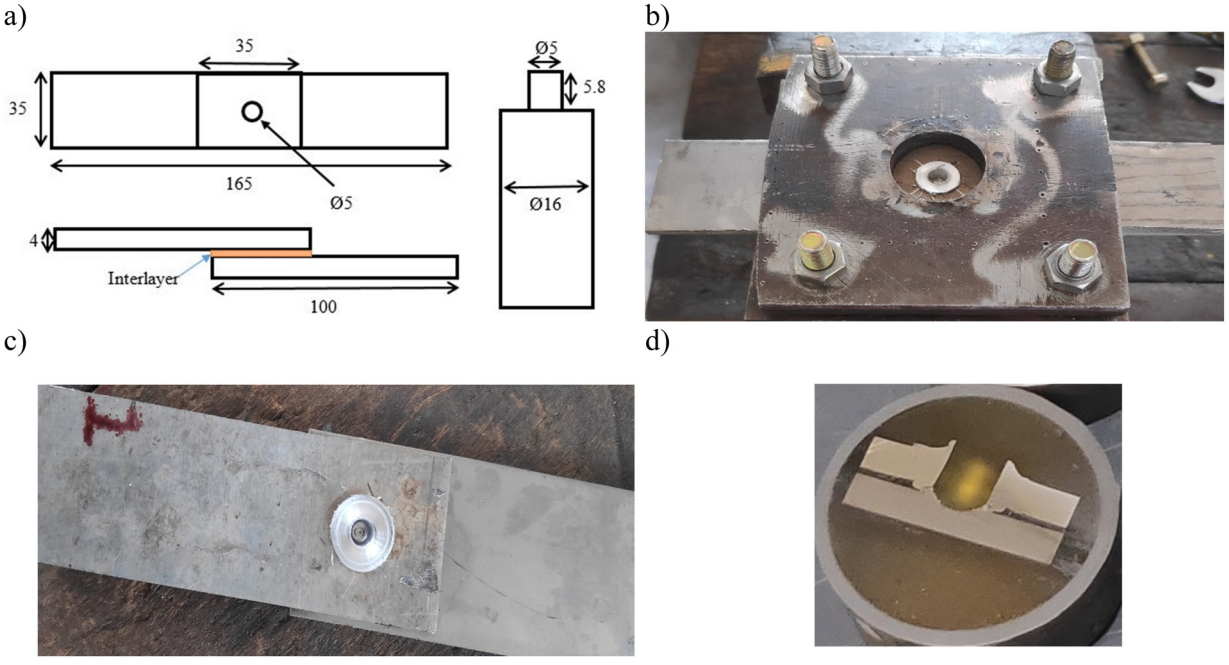

Figure 2: (a) Schematic of lap joint and friction stir spot tool (mm), (b) specimen holder, (c) welded sample, and (d) sample for microstructural analysis.

The tensile shear load test was conducted by using universal testing machine (INSTRON 3385H). Specimens were mounted between the jaws, and the load rate was constant with cross head speed of 3 mm/min at ambient temperature for all specimens. Three identical specimens were prepared at each welding parameter. For weld characterization, samples were cut through the center of the weld joint (by using DK 7763 EDM wire cut machine) parallel to the loading direction. After the cutting process, specimens were mounted by using the cold mount method. In this method, 50% epoxy hardener and 50% epoxy resins were mixed together and then poured into the specimen. All mounted specimen's passes through grinding and polishing processes to obtain mirror face surface. Grinding of all specimens was accomplished by using various numbers of sand papers (220, 320, 500, 1,000, 2,400, and 4,000) to obtain abrasive-free surface. After grinding, all specimens were washed using distilled water. Distilled clean specimen was subjected to the polishing process by using 1 µm grit size particle-impregnated carrier paste until mirror face surface is obtained. To reveal the microstructure of the weld coupons, the samples were etched with the killer reagent H_2O (95 mL) + HNO_3 (2.5 mL) + HCL (1.5 mL) + HF (1 mL). Samples for the micro-hardness test were prepared according to the ASTM E384 standard test method [53]. The micro-hardness values of all experiments were measured by using Vickers test machine (Tukon micro-hardness tester) with Vickers hardness of 0.5 HV at force of 4.903 N at dwell time of 20 s. Multiple indents were made along the cross-section of the weld joint (Figure 2d). Microstructural analysis was conducted by using stereo and optical microscope. Low magnification stereo microscope was used to observe the cross-sectional of the weld joint Figure 6. Olympus optical microscope was used to evaluate the internal structure and micro-cracks of the weld joint at the interface (Figure 7).

3 Result and discussion

3.1 Temperature evaluation

The elevated temperature plays a dominant role in the plastic flow of materials and diversified mixing during the FSSW process of dissimilar metal alloys, as well as the temperature plays a key role in nucleation of IMCs and the growth of these compound because the process of IMC is thermally activated [54]. Thus, the study of thermal history of dissimilar metal alloys during the FSSW welding process has significant importance. In this study, the thermal cycles of two dissimilar metal alloys were measured at the top and the bottoms of sheets. The temperature of these points is based to the selected parameters (rotational speeds and dwell times). The peek temperatures at the rotational speed of 2,000 rpm at the top sheet were 333.8 and 305.5°C at dwell time of 10 and 5 s respectively. The peak temperature was obtained in aluminum plates (Figure 3). The obtained results indicate that high rotational speed led to high heat input that leads to the peak temperature [55]. As the rotational speed increases with respect to the dwell time, temperature increases accordingly in both dwell times. As stated by Goushegir *et al.* [44] in AA2024-T3 with CF-PPS joint fabricated by friction spot welding, the average obtained peak temperature was between 350 and 400°C. The thermal degradation range of the polymer in the CF-PPS is well below this temperature. As the rotational

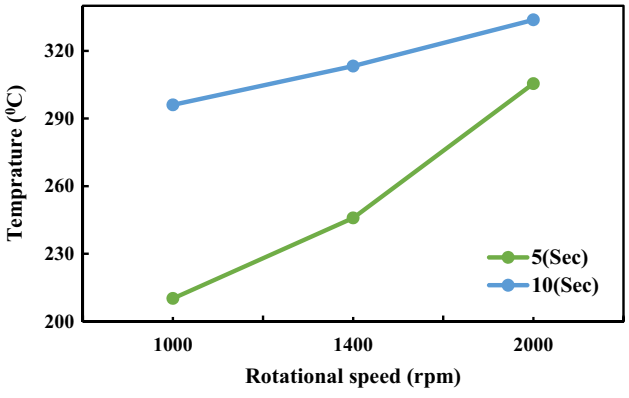

Figure 3: Temperature evaluation of Al7075-T651/Ti-6Al-4V alloy at different rotational speeds and dwell times.

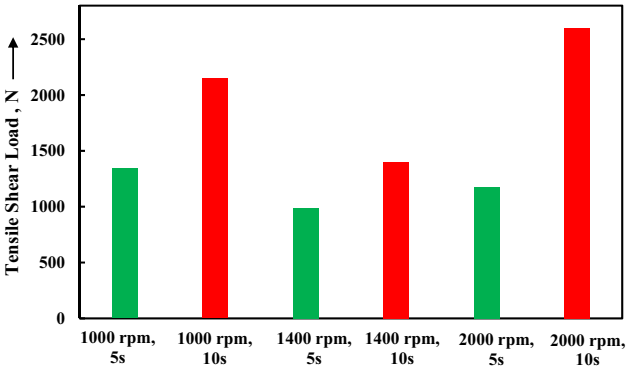

Figure 4: Variation in tensile shear load of FSSW joint as a function of rotational speed and dwell time.

speed increases, the value of peak temperature increases from 40 to 50°C during the welding process.

3.2 Tensile shear load

The effect of welding parameters on tensile shear load was evaluated by manipulating the rotational speed and dwell time (Figure 4). It has been observed from the previous literature that in dissimilar FSSW welding of aluminum and titanium alloys without interlayer at high rotational speed and high dwell time, the tensile shear load was depreciated. However, with CFRP interlayer, this scenario is totally opposite and maximum tensile shear load was obtained at high rotational speed and high dwell time. At the dwell time of 10 s, the maximum tensile shear load value of the weld joints were 2597.8 and 2147.6 N cross ponding to their rotational speed 2,000 and 1,000 rpm, respectively. At the rotational speed of 2,000 rpm, tensile shear load value was enhanced by 17.3%. Increment in the rotational speed resulted in high plastically deformation zone (PDZ) area due to higher heat input [56]. Between the two plates, high heat input larger PDZ area causes higher adhesion force, which tends to increase the tensile shear load of the joints (see Figure 7d) [44]. Also, high rotational speed and high dwell time generate high heat, which decrease the viscosity of the interlayer; therefore, certain amount of molten interlayer CFRP squeezed out of bonding area as flash during this joining, which tend to establish a sound weld joint. High dwell time improves the joint length, and also high dwell time increases temperature, which increases the volume of the stirring material under the tool that leads to improve the tensile shear load [57]. The second high tensile shear load was obtained at the rotational speed of 1,000 rpm and 10 s of dwell time. Heat generation at 1,000 rpm was lower than 1,400 and 2,000 rpm. However, longer dwell time of 10 s plays an important role in improving the grain structure (grain size) and the joint length of the weld interface, which increase the tensile shear load. High dwell time led to high tensile shear load [58].

However, a low tensile shear load value of 1403.4 N was obtained at the rotational speed of 1,400 rpm and 10 s dwell time due to heat generation, which resulted in the initiation micro-cracks in the periphery of the stir zone of the joint, thereby reducing the tensile shear load. The bond width in dissimilar aluminum-titanium alloy at the hook region plays a significant role in the tensile shear load [32]. According to Aydin *et al.* [59], lower tensile shear load is due to lower precipitate free zone (PFZ) along the grain boundaries emerged from the over aging effect with higher heat input owing to the higher dwell time. The weld with higher tensile shear load exhibits both brittle and ductile behaviors, while the joint with low tensile shear load value exhibits only brittle behavior [60].

At shorter dwell time of 5 s, the peak tensile shear load results were 1343.3, 986.4, and 1173.3 N at rotational speeds of 1,000, 1,400 and 2,000 rpm, respectively. The revealed results demonstrate that at low rotational speed and low dwell time, high tensile shear load increased compared to other process parameters, as the rotational speed increases, a drop in the tensile shear load was observed at the rotational speed of 1,400 and 2,000 rpm, which was mainly due to lower dwell time. Soften material did not gain enough time to stir and mixed very well at the interface of the weld joint and creates micro-cracks and IMC, which fairly depreciates the tensile shear load

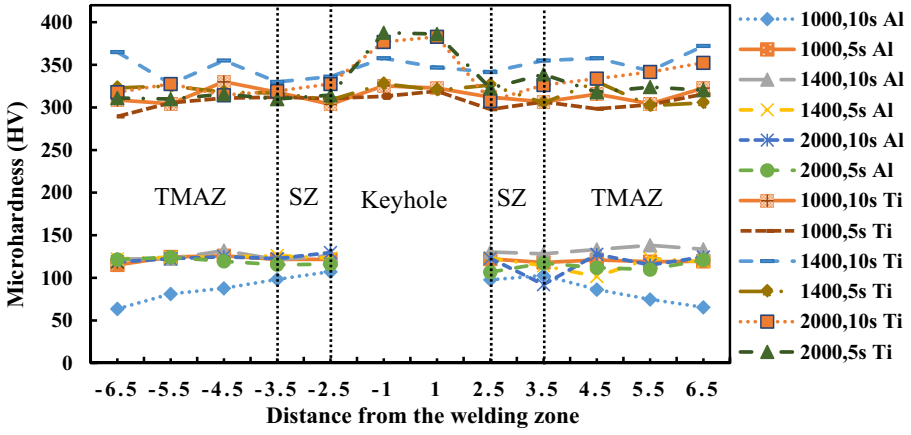

Figure 5: Micro-hardness values of weld interface at different rotational speeds and dwell times.

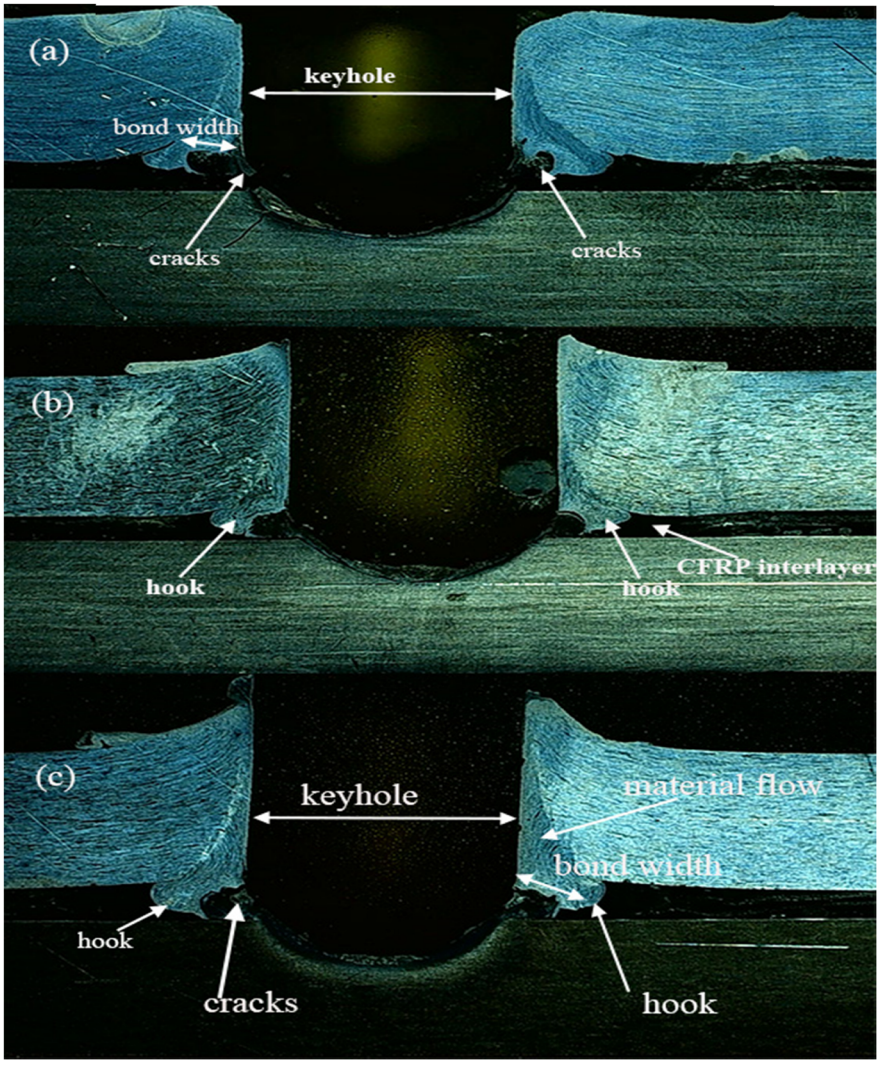

Figure 6: Cross-sectional view of FSSW joint with carbon fiber (a) 1,000 rpm and 5 s dwell time, (b) 1,400 rpm and 10 s dwell time, and (c) 1,400 rpm and 5 s dwell time.

(Figure 7(b and c)) [41]. In FSSW of CFRP joint, three primary bonding mechanisms were founded by ref. [61]: at the interface, macro-mechanical interlocking formed during insertion from aluminum sheet to the composite layer, micromechanical interlocking because of the keying effect of aluminum and fiber entrapment, and finally adhesion forces between consolidated molten fiber interlayer and aluminum. This material mixing phenomena in aluminum/CFRP welding were observed by ref. [62], which led increase or decrease of the strength of the lap shear joint with the variation of parameters. Dwell time plays a vital role in the improvement of the tensile shear load. The effect of dwell time was clearly observed at the rotational speed of 2,000 rpm with 54.75% improvement in tensile shear load obtained from shorter dwell 5 s to higher dwell time of 10 s.

3.3 Micro-hardness

Figure 5 shows the micro-hardness profile of dissimilar Al 7075-T651 and Ti-6Al-4V with CFRP interlayer welded joints made at dwell time of 5 and 10 s and the rotational speed of 1,000, 1,400, and 2,000 rpm. Micro-hardness test was carried out after 40 days natural aging. The hardness profile of the weld joint in Al 7075-T651 side exhibits the smooth trend in the thermomechanical affected zone and the stir zone. A minor increase in hardness values was observed in some samples of stir zone areas. Moreover, rotational speed and dwell time imply a significant effect on hardness value. Especially at the rotational speed of 1,000 rpm and dwell time of 10 s, micro-hardness was very low in the thermomechanical affected zone and gradually increases until the stir zone region. The

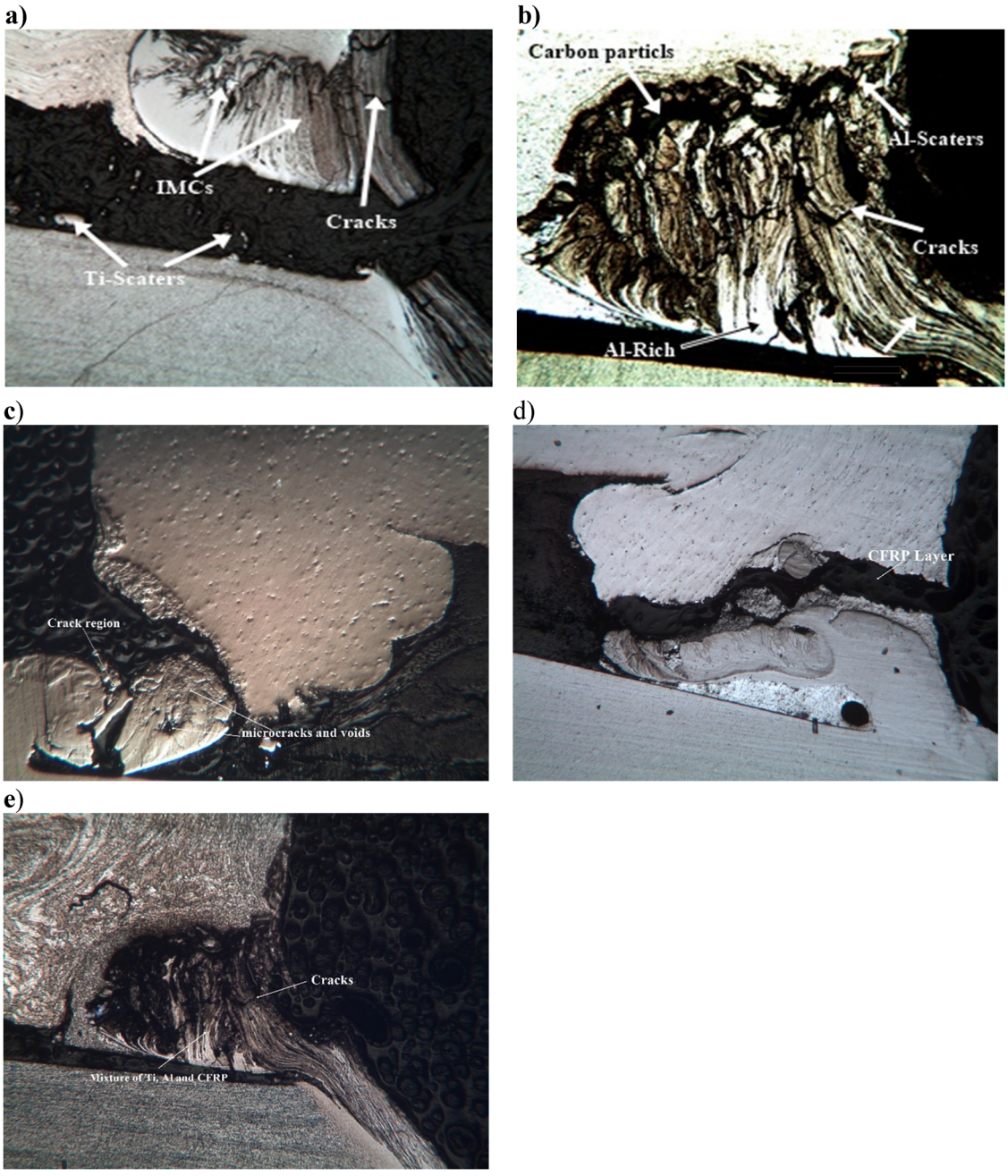

Figure 7: Optical microscopic results (a) 1,000 rpm 5 s, (b) 1,400 rpm 5 s, (c) 2,000 rpm 5 s, (d) 2,000 rpm 10 s, and (e) 1,400 rpm 10 s.

hardness results at shorter dwell time of 5 s were higher than 10 s dwell at rotational speed of 1,000 rpm [63]. The maximum hardness value in AA7075-T651 was obtained at 1,400 rpm at dwell time of 10 s. The hardness values of thermomechanical affected zone were higher than the stir zone due to grain size increment. The stir zone and thermomechanical affected zone are affected by thermomechanical parameters of welding, which include maximum temperature, cooling rate, and deformation [57]. Totally, the opposite trend of hardness result was observed at high rotational speeds of 1,400 and 2,000 rpm compared to the low rotational speed of 1,000 rpm. Higher hardness values were obtained at high dwell time 10 s compared to that at low dwell time of 5 s.

In Ti-6Al-4V alloy, maximum hardness values of 387.7 and 386.1 HV were obtained under the tool pin region at the rotational speed of 2,000 rpm at dwell time of 5 and 10 s, respectively. There is a minor difference in hardness between 5 and 10 s dwell time. The hardness values were higher under hook of the tool due

to the dynamic recrystallization at high temperature, which causes severe plastic deformation [64]. At the rotational speed of 1,400 rpm and dwell time of 10 s, a sharp increment in hardness was observed in the thermomechanical affected zone region. The improvement in hardness is due to IMC, which causes the material to behave brittle [65]. FSSW joint exhibits various microstructural zones from the periphery of keyhole toward the base metal, dynamically recrystallized zone (stir zone), thermo-mechanical affected zone and base metal [66]. Tool rotational speed and dwell time have direct effect on the temperature of the weld joint [57].

3.4 Microstructural analysis

Figure 6 shows the cross-sectional view of welded specimens at different welding parameters evaluated by stereo and optical microscopy. A keyhole is formed due to the withdrawal of the tool after the formation of a weld joint. Two identical weld zones formed at the both sides of the keyhole. In Figure 6(a–c), a partially bonded region called hook is found [67]. It is the geometric defect, which is formed due to the insufficient metallurgical bonding between two sheets [68]. It has been reported that the plunge speed has also effect on hook geometry and tensile shear load of a weld joint [69]. In the conventional FSSW joint, the distance from the keyhole to the tip of the hook in the interface of a joint (including stir zone and hook region) is addressed as the bond width of the weld [70]. The bond width shows the minimum distance between the hook tip and pinhole boundary (Figure 6). The size of the bond width vary at each welding parameters, and also the size of hook region (stir zone and bonded width) [68] increased by increasing the dwell time of the weld joint. Upward material flow increases as the rotational speed increase (Figure 6c). High rotational speed during penetration of a tool pin and dwell time provides a driving force to material to move upward [71]. In the interface of the weld joint, micro-crack is observed along the keyhole. Micro-crack is formed due to incongruous deformation during the cooling process because of variation in the thermal expansion coefficient [72]. Residual stress also significantly affect the weld quality [73]. Aluminum and titanium alloys have low intersolubility during welding and produce brittle IMC, which easily propagate micro-crack at the weld interface, and reduce the tensile shear load of the weld joint [74].

The Al/Ti dissimilar metal hybrid structure has numerous benefits compared to single material to fulfill the requirement of both performance and lightweight. Since in thermal welding, the inter solubility of aluminum and titanium is low, brittle intermetallic easily can form interface cracks, see Figure 7(a and b), which severely degrades the mechanical properties of Al/Ti welded joints [74]. Some additional irregularities were also observed in the near hook periphery due to the propagation of micro-cracks and nonuniform mixing of a material during the welding process. Crack propagation is because of IMC, which is formed at the weld interface [75]. Hook always acts as a failure source of the weld joint. Therefore, we contemplate that the first crack starts from the hook (Figure 6) and then breed through the IMC layer [76]. Both aluminum and titanium are active elements, which formed $AlTi_3$ [77] and Ti-Al-C (see Figure 9) [78], and

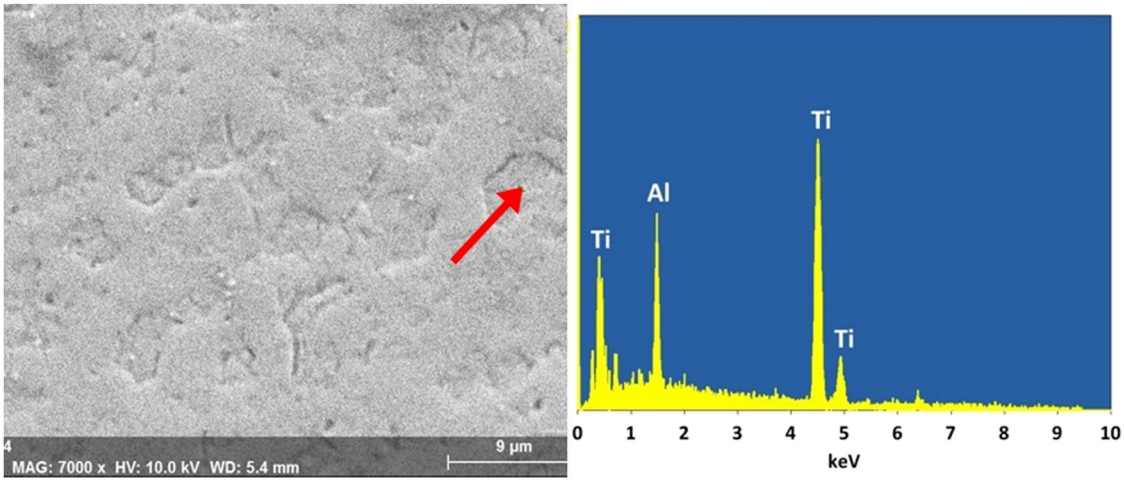

Figure 8: SEM-EDS analysis of friction stir spot welded joint: 2,000 rpm and 5 s dwell time.

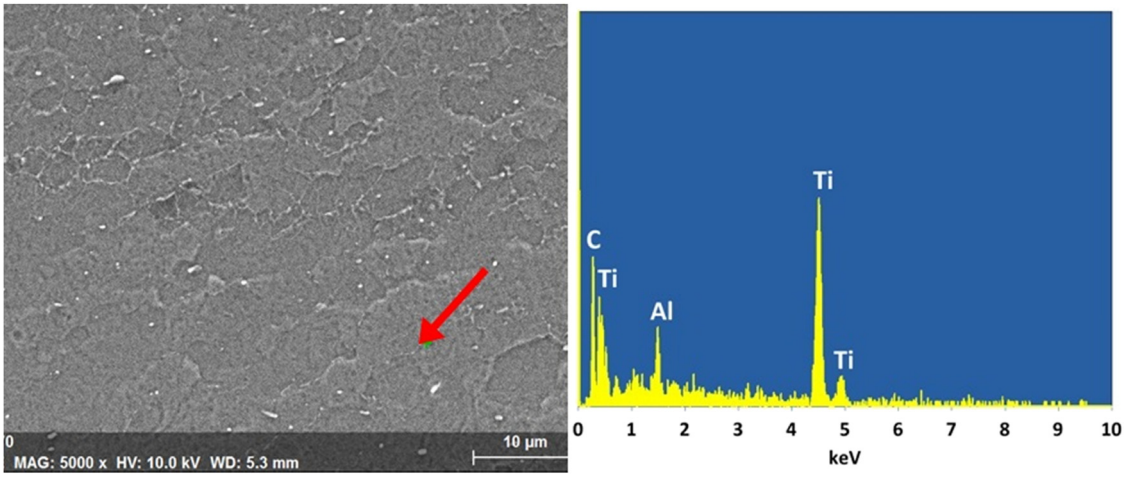

Figure 9: SEM-EDS analysis of friction stir spot welded joint: 2,000 rpm and 5 s dwell time.

other IMCs depends on the titanium-aluminum duality phase diagram [79]. Generally, in dissimilar welding of Al/Ti alloys, the strength of the joint relays on the formation and distribution of IMCs [80].

This article (SEM-EDS) analyzed the tool rotational speed of 2,000 rpm and dwell time of 5 s. Dissimilar metal alloys made a strong joint with the CFRP interlayer. According to Kattner *et al.* [81], the formation of IMC depends on the function of temperature in the Ti-Al binary system. At high tensile shear load weld joint, the maximum temperature was 333.8°C. In Figure 8, Ti_3Al IMC is seen, which is formed due to the large amount of Ti fragments. Increment in rotational speed increase the amount of Ti fragments in the weld interface which formed Ti_3Al IMC, due to that cracks initiated in the interface of the weld joint causes to reduce the tensile shear load. Also the thickness of IMC increased with the increasing of the rotational speed [41]. Cracks are shown in Figure 7, and the bonded regions are mainly formed in the aluminum side, which is denoted as hook. The flow of titanium toward aluminum makes reaction with aluminum, which produces Ti_3Al IMC [82]. However, aluminum carbide Al_4C_3 was not formed due to the low heat input (Max 333.8°C) during the welding process.

Ti and Al are considered very appropriate materials as they provide sustainable strength to weight ratio and volume reduction. But when reacted with composite at the elevated temperature, they show high hardness and wear resistance [83]. Carbon fiber owes high modulus that exhibits good chemical compatibility with the Ti-Al compound. Therefore, carbon fibers may be good reinforcements of Ti-Al intermetallic [84]. Furthermore, the phase diagram of ternary Ti-Al-C IMC confirms the solubility of carbon in the α_2 phase, which is higher than in the γ phase [85]. Figure 9 shows ternary (Ti-Al-C) IMC, in which carbon comes from the CFRP interlayer, and the mixing of these element occurred due to the high heat input during the FSSW process. Due to the presence of carbon reinforcement in the (Ti-Al-C) compound, the hardness increased by 18.90% in the keyhole of joint rather than in the stir zone and the thermal mechanical affected zone [86]. The presence of more carbon fiber as reinforcement will increase micro-hardness. The addition of carbonaceous particles can improve the strength-to-weight ratio [83]. Also, excessive amount of carbon reduces the distance between aluminum and fiber and increases stress, which reduce the strength of the composite [87]. In ternary Ti-Al-C IMC, carbon with titanium acts as a nucleation site during solidification and thus refines the grain size, which might improve the joint strength [88].

4 Conclusion

In this present study, Al 7075-T651/Ti-6Al-4V alloy with CFRP as an interlayer was used to make a joint by the FSSW process. The effect of welding parameters such as rotational speed and dwell time on mechanical and microstructural properties was studied. Based on experimental results, the following conclusion are made.

- The maximum tensile shear load of 2597.8 N was obtained at the rotational speed of 2,000 rpm and dwell time of 10 s, which is 54.75% higher than shorter dwell time 5 s at the same rotational speed. The increase of the tensile shear load is due to heat input that melt the CFRP interlayer that squeezed out of the center, which enhances the bonding strength of the joint.

- The minimum tensile shear load value of 986.4 N increased at the rotational speed of 1,400 rpm at 5 s dwell time. As dwell time increases to 10 s, the tensile shear load values increased by 29.7%, which shows that the dwell time has a significant effect on the tensile shear load. Considerable irregularities (micro-cracks) were observed at the rotational speed of 1,400 rpm, which might be due to dynamic recrystallization of weld joint.
- The hardness value was mainly affected by the tool rotational speed. The maximum hardness value was achieved at the high rotational speed of 2,000 rpm and 5 s dwell time. The increase in hardness was due to the presence of ternary Ti-Al-C IMC. In aluminum side, high hardness was obtained at 1,400 rpm and 10 s dwell time. Higher hardness value causes to decrease the tensile shear load of a weld joint.
- Scanning electron microscopy coupled with energy-dispersive spectroscopy shows the formation of Ti_3Al and Ti-Al-C intermetallic compound, which affects the tensile shear load of a weld joint. The formation of IMC depends on the heat cycle of a weld joint, which can be controlled by the welding parameter (rotational speed and dwell time) of the FSSW process.

Funding information: The authors state no funding involved.

Author contributions: All authors have accepted responsibility for the entire content of this manuscript and approved its submission.

Conflict of interest: The authors state no conflict of interest.

References

[1] Connolly C. Friction spot joining in aluminium car bodies. Ind Robot Int J. 2007;34:17–20.
[2] Bozzi S, Helbert-Etter AL, Baudin T, Klosek V, Kerbiguet JG, Criqui B. Influence of FSSW parameters on fracture mechanisms of 5182 aluminium welds. J Mater Process Technol. 2010;210:1429–35.
[3] Hancock R. Friction welding of aluminum cuts energy costs by 99%. Welding J. 2004;83:40–3.
[4] Salih OS, Ou H, Wei X, Sun W. Microstructure and mechanical properties of friction stir welded AA6092/SiC metal matrix composite. Mater Sci Eng A. 2019;742:78–88.
[5] Cinar Z, Asmael M, Zeeshan Q, Safaei B. Effect of springback on A6061 sheet metal bending: a review. J Kejuruteraan. 2021;33:13–26.
[6] Yu T, Soomro SA, Huang F, Wei W, Wang B, Zhou Z, et al. Naturally or artificially constructed nanocellulose architectures for epoxy composites: a review. Nanotechnol Rev. 2020;9:1643–59.
[7] Park OK, Kim SG, You NH, Ku BC, Hui D, Lee JH. Synthesis and properties of iodo functionalized graphene oxide/polyimide nanocomposites. Compos B Eng. 2014;56:365–71.
[8] Park J, Oh M, Hossain A, Lee KY, Yoo D, Kim Y, et al. Mechanical properties of individual nanorods and nanotubes in forest-like structures. Scr Mater. 2017;133:54–8.
[9] Jambor A, Beyer M. New cars-new materials. Mater Des. 1997;18:203–9.
[10] Karbalaei Akbari M, Baharvandi HR, Mirzaee O. Fabrication of nano-sized Al_2O_3 reinforced casting aluminum composite focusing on preparation process of reinforcement powders and evaluation of its properties. Compos B Eng. 2013;55:426–32.
[11] Behdinan K, Moradi Dastjerdi R, Safaei B, Qin Z, Chu F, Hui D. Graphene and CNT impact on heat transfer response of nanocomposite cylinders. Nanotechnol Rev. 2020;9:41–52.
[12] Talebizadehsardari P, Eyvazian A, Asmael M, Karami B, Shahsavari D, Mahani RB. Static bending analysis of functionally graded polymer composite curved beams reinforced with carbon nanotubes. Thin-Walled Struct. 2020;157:107139.
[13] Gao W, Qin Z, Chu F. Wave propagation in functionally graded porous plates reinforced with graphene platelets. Aerosp Sci Technol. 2020;102:105860.
[14] Sahmani S, Safaei B. Large-amplitude oscillations of composite conical nanoshells with in-plane heterogeneity including surface stress effect. Appl Math Modell. 2021;89:1792–813.
[15] Geng D, Teng Y, Liu Y, Shao Z, Jiang X, Zhang D. Experimental study on drilling load and hole quality during rotary ultrasonic helical machining of small-diameter CFRP holes. J Mater Process Technol. 2019;270:195–205.
[16] Asmael M, Safaei B, Zeeshan Q, Zargar O, Nuhu AA. Ultrasonic machining of carbon fiber–reinforced plastic composites: a review. Int J Adv Manuf Tech. 2021;113:3079–120.
[17] Liu Y, Qin Z, Chu F. Nonlinear forced vibrations of functionally graded piezoelectric cylindrical shells under electric-thermo-mechanical loads. Int J Mech Sci. 2021;201:106474.
[18] Casavola C, Palano F, De Cillis F, Tati A, Terzi R, Luprano V. Analysis of CFRP joints by means of T-pull mechanical test and ultrasonic defects detection. Materials. 2018;11:620.
[19] Han J, Wang D, Zhang P. Effect of nano and micro conductive materials on conductive properties of carbon fiber reinforced concrete. Nanotechnol Rev. 2020;9:445–54.
[20] Bhat A, Budholiya S, Aravind Raj S, Sultan MTH, Hui D, Md Shah AU, et al. Review on nanocomposites based on aerospace applications. Nanotechnol Rev. 2021;10:237–53.
[21] Jeong Y, Kim W, Gribniak V, Hui D. Fatigue Behavior of concrete beams prestressed with partially bonded CFRP bars subjected to cyclic loads. Material (Basel). 2019;12:3352.
[22] Marsh G. Composites and metals – a marriage of convenience. Reinf Plast. 2014;58:38–42.
[23] Lin S, Jia X, Sun H, Sun H, Hui D, Yang X. Thermo-mechanical properties of filament wound CFRP vessel under hydraulic and atmospheric fatigue cycling. Compos B Eng. 2013;46:227–33.
[24] Song Z, Nakata K, Wu A, Liao J, Zhou L. Influence of probe offset distance on interfacial microstructure and mechanical

properties of friction stir butt welded joint of Ti6Al4V and A6061 dissimilar alloys. Mater Des. 2014;57:269–78.
[25] Zhang Z, Yang X, Zhang J, Zhou G, Xu X, Zou B. Effect of welding parameters on microstructure and mechanical properties of friction stir spot welded 5052 aluminum alloy. Mater Des. 2011;32:4461–70.
[26] Xu RZ, Ni DR, Yang Q, Liu CZ, Ma ZY. Pinless friction stir spot welding of Mg–3Al–1Zn alloy with Zn interlayer. J Mater Sci Technol. 2016;32:76–88.
[27] Manladan SM, Yusof F, Ramesh S, Fadzil M. A review on resistance spot welding of magnesium alloys. Int J Adv Manuf Tech. 2016;86:1805–25.
[28] Chen T. Process parameters study on FSW joint of dissimilar metals for aluminum–steel. J Mater Sci. 2009;44:2573–80.
[29] Ahmad R, Asmael MBA. Effect of aging time on microstructure and mechanical properties of AA6061 friction stir welding joints. Int J Automot Mech Eng. 2015;11:2364.
[30] Labus Zlatanovic D, Balos S, Bergmann JP, Köhler T, Grätzel M, Sidjanin L, et al. An experimental study on lap joining of multiple sheets of aluminium alloy (AA 5754) using friction stir spot welding. Int J Adv Manuf Tech. 2020;107:3093–107.
[31] Bozkurt Y. The optimization of friction stir welding process parameters to achieve maximum tensile strength in polyethylene sheets. Materials Design. 2012;35:440–45.
[32] Zhou X, Chen Y, Li S, Huang Y, Hao K, Peng P. Friction stir spot welding-brazing of Al and hot-dip aluminized Ti alloy with Zn interlayer. Met. 2018;8:922.
[33] Zhang Y, Zhou J, Sun D, Gu X. Nd:YAG laser welding of dissimilar metals of titanium alloy to stainless steel without filler metal based on a hybrid connection mechanism. J Mater Res Technol. 2020;9:1662–72.
[34] Hynes NRJ, Velu PS. Effect of rotational speed on Ti-6Al-4V-AA 6061 friction welded joints. J Manuf Process. 2018;32:288–97.
[35] Nasir T, Asmaela M, Zeeshana Q, Solyalib D. Applications of machine learning to friction stir welding process optimization. J Kejuruteraan. 2020;32:171–86.
[36] Wang T, Upadhyay P, Reza-E-Rabby M, Li X, Li L, Soulami A, et al. Joining of thermoset carbon fiber reinforced polymer and AZ31 magnesium alloy sheet via friction stir interlocking. Int J Adv Manuf Tech. 2020;109:689–98.
[37] Nasir T, Kalaf O, Asmael M. Effect of rotational speed, and dwell time on the mechanical properties and microstructure of dissimilar AA5754 and AA7075-T651 aluminum sheet alloys by friction stir spot welding. Mater Sci. 2021
[38] Hynes NRJ, Velu PS, Nithin AM. Friction push plug welding in airframe structures using Ti-6Al-4V plug. J Braz Soc Mech Sci Eng. 2018;40:158.
[39] Plaine AH, Suhuddin UFH, Afonso CRM, Alcântara NG, dos Santos JF. Interface formation and properties of friction spot welded joints of AA5754 and Ti6Al4V alloys. Mater Des. 2016;93:224–31.
[40] Chen YC, Nakata K. Microstructural characterization and mechanical properties in friction stir welding of aluminum and titanium dissimilar alloys. Mater Des. 2009;30:469–74.
[41] Choi J-W, Liu H, Fujii H. Dissimilar friction stir welding of pure Ti and pure Al. Mater Sci Eng A. 2018;730:168–76.
[42] Cheepu M, Muthupandi V, Che WS. Improving mechanical properties of dissimilar material friction welds. Appl Mech Mater. 2018;877:157–62.
[43] Cao X, Shi Q, Liu D, Feng Z, Liu Q, Chen G. Fabrication of in situ carbon fiber/aluminum composites via friction stir processing: Evaluation of microstructural, mechanical and tribological behaviors. Compos B Eng. 2018;139:97–105.
[44] Goushegir SM, dos Santos JF, Amancio-Filho ST. Friction spot joining of aluminum AA2024/carbon-fiber reinforced poly(phenylene sulfide) composite single lap joints: microstructure and mechanical performance. Mater Des. 2014;54:196–206.
[45] Esteves JV, Goushegir SM, dos Santos JF, Canto LB, Hage E, Amancio-Filho ST. Friction spot joining of aluminum AA6181-T4 and carbon fiber-reinforced poly(phenylene sulfide): effects of process parameters on the microstructure and mechanical strength. Mater Des. 2015;66:437–45.
[46] Ageorges C, Ye L. Resistance welding of metal/thermoplastic composite joints. J Thermoplast Compos Mater. 2016;14:449–75.
[47] André NM, Goushegir SM, Santos JF, Canto LB, Amancio-Filho ST. On the microstructure and mechanical performance of Friction Spot Joining with additional film interlayer. Proceedings of the annual technical conference of society of plastics engineers (ANTEC 2014). USA: Society of Plastics Engineers; 2014. p. 1791–97.
[48] Madhusudhan Reddy G, Venkata Ramana P. Role of nickel as an interlayer in dissimilar metal friction welding of maraging steel to low alloy steel. J Mater Process Technol. 2012;212:66–77.
[49] Shojaei Zoeram A, Akbari Mousavi SAA. Effect of interlayer thickness on microstructure and mechanical properties of as welded Ti6Al4V/Cu/NiTi joints. Mater Lett. 2014;133:5–8.
[50] Xu RZ, Ni DR, Yang Q, Liu CZ, Ma ZY. Influencing mechanism of Zn interlayer addition on hook defects of friction stir spot welded Mg–Al–Zn alloy joints. Mater Des. 2015;69:163–69.
[51] Kalaf O, Nasir T, Asmael M, Safaei B, Zeeshan Q, Motallebzadeh A, et al. Friction stir spot welding of AA5052 with additional carbon fiber-reinforced polymer composite interlayer. Nanotechnol Rev. 2021;10:201–9.
[52] Japanese Industrial Standard. Method of tension shear test for spot welded joint. Japan: Japanese Standard Association, JIS Z 3136; 1999. p. 637–9.
[53] Standard A. E384, Standard test method for microindentation hardness of materials. West Conshohocken, PA: ASTM International; 2000.
[54] Abdollah-Zadeh A, Saeid T, Sazgari B. Microstructural and mechanical properties of friction stir welded aluminum/copper lap joints. J Alloys Compd. 2008;460:535–38.
[55] Zhou L, Li GH, Zhang RX, Zhou WL, He WX, Huang YX, et al. Microstructure evolution and mechanical properties of friction stir spot welded dissimilar aluminum-copper joint. J Alloys Compd. 2019;775:372–82.
[56] Zamani SMM, Behdinan K, Razfar MR, Fatmehsari DH, Mohandesi JA. Studying the effects of process parameters on the mechanical properties in friction stir welding of Al-SiC composite sheets. Int J Adv Manuf Tech. 2021;113:3629–41.
[57] Farmanbar N, Mousavizade SM, Elsa M, Ezatpour HR. AA5052 sheets welded by protrusion friction stir spot welding: High mechanical performance with considering sheets thickness at low dwelling time and tool rotation speed. Proc Inst Mech Eng Part C J Mech Eng Sci. 2019;233:5836–47.
[58] Farmanbar N, Mousavizade SM, Ezatpour HR. Achieving special mechanical properties with considering dwell time of

AA5052 sheets welded by a simple novel friction stir spot welding. Mar struct. 2019;65:197–214.
[59] Aydin H, Tuncel O, Tutar M, Bayram ALI. Effect of tool pin profile on the hook geometry and mechanical properties of a friction stir spot welded AA6082-T6 aluminum alloy. Trans Can Soc Mech Eng. 2020;45(2):233–48.
[60] Manickam S, Rajendran C, Balasubramanian V. Investigation of FSSW parameters on shear fracture load of AA6061 and copper alloy joints. Heliyon. 2020;6:e04077.
[61] Goushegir SM. Friction spot joining (FSpJ) of aluminum-CFRP hybrid structures. Weld World. 2016;60:1073–93.
[62] André NM, Goushegir SM, dos Santos JF, Canto LB, Amancio-Filho ST. Friction Spot Joining of aluminum alloy 2024-T3 and carbon-fiber-reinforced poly(phenylene sulfide) laminate with additional PPS film interlayer: Microstructure, mechanical strength and failure mechanisms. Compos B Eng. 2016;94:197–208.
[63] Fujimoto M, Inuzuka M, Koga S, Seta Y. Development of friction spot joining. Weld World. 2005;49:18–21.
[64] Rosendo T, Parra B, Tier MAD, da Silva AAM, dos Santos JF, Strohaecker TR, et al. Mechanical and microstructural investigation of friction spot welded AA6181-T4 aluminium alloy. Mater Des. 2011;32:1094–100.
[65] Piccini JM, Svoboda HG. Effect of pin length on friction stir spot welding (FSSW) of dissimilar aluminum-steel joints. Procedia Mater Sci. 2015;9:504–13.
[66] Yang Q, Mironov S, Sato YS, Okamoto K. Material flow during friction stir spot welding. Mater Sci Eng A. 2010;527:4389–98.
[67] Badarinarayan H, Shi Y, Li X, Okamoto K. Effect of tool geometry on hook formation and static strength of friction stir spot welded aluminum 5754-O sheets. Int J Mach Tools Manuf. 2009;49:814–23.
[68] Rana PK, Narayanan RG, Kailas SV. Assessing the dwell time effect during friction stir spot welding of aluminum polyethylene multilayer sheets by experiments and numerical simulations. Int J Adv Manuf Tech. 2021;114:1953–73.
[69] Song X, Ke L, Xing L, Liu F, Huang C. Effect of plunge speeds on hook geometries and mechanical properties in friction stir spot welding of A6061-T6 sheets. Int J Adv Manuf Tech. 2014;71:2003–10.
[70] Rao HM, Yuan W, Badarinarayan H. Effect of process parameters on mechanical properties of friction stir spot welded magnesium to aluminum alloys. Mater Des. 2015;66:235–45.
[71] Yin YH, Sun N, North TH, Hu SS. Hook formation and mechanical properties in AZ31 friction stir spot welds. J Mater Process Technol. 2010;210:2062–70.
[72] Li GH, Zhou L, Shu FY, Liu YC. Statistical and metallurgical analysis of dissimilar friction stir spot welded aluminum/copper metals. J Mater Eng Perform. 2020;29:1830–40.
[73] Glaissa MAA, Asmael M, Zeeshan Q. Recent applications of residual stress measurement techniques for FSW Joints. A J Kejuruteraan. 2020;32:357–71.
[74] Xue X, Pereira A, Vincze G, Wu X, Liao J. Interfacial characteristics of dissimilar Ti6Al4V/AA6060 lap joint by pulsed Nd:YAG laser welding. Met. 2019;9:71.
[75] Chen Y, Liu C, Liu G. Study on the joining of titanium and aluminum dissimilar alloys by friction stir welding. The Open Mater Sci J. 2011;5:256–61.
[76] Dong Z, Song Q, Ai X, Lv Z. Effect of joining time on intermetallic compound thickness and mechanical properties of refill friction stir spot welded dissimilar Al/Mg alloys. J Manuf Process. 2019;42:106–12.
[77] Li P, Lei Z, Zhang X, Chen Y. Effects of a post-weld heat treatment on the microstructure and mechanical properties of dual-spot laser welded-brazed Ti/Al butt joints. J Manuf Process. 2021;61:492–506.
[78] Liu ZG, Guo JT, Ye LL, Li GS, Hu ZQ. Formation mechanism of TiC by mechanical alloying. Appl Phys Lett. 1994;65:2666–68.
[79] Batalu D, Cosmeleata G, Aloman A. Critical analysis of the Ti-Al phase diagrams. UPB Sci Bull Ser B Chem Mater Sci. 2006;68:77–90.
[80] Liu K, Li Y, Wei S, Wang J. Interfacial microstructural characterization of Ti/Al joints by gas tungsten arc welding. Mater Manuf Processes. 2014;29:969–74.
[81] Kattner UR, Lin JC, Chang YA. Thermodynamic assessment and calculation of the Ti-Al system. Metall Mater Trans A. 1992;23A:2081–90.
[82] Asmael MBA, Glaissa MAA. Effects of rotation speed and dwell time on the mechanical properties and microstructure of dissimilar aluminum-titanium alloys by friction stir spot welding (FSSW). Materialwiss Werkstofftech. 2020;51:1002–08.
[83] Fereiduni E, Ghasemi A, Elbestawi M. Selective laser melting of aluminum and titanium matrix composites: recent progress and potential applications in the aerospace industry. Aerosp. 2020;7:77.
[84] Cortés P, Cantwell WJ. The prediction of tensile failure in titanium-based thermoplastic fibre–metal laminates. Compos Sci Technol. 2006;66:2306–16.
[85] Agne MT, Anasori B, Barsoum MW. Reactions between Ti_2AlC, B4C, and Al and Phase Equilibria at 1000°C in the Al–Ti–B–C Quaternary System. J Phase Equilibria Diffus. 2015;36:169–82.
[86] Chandran P, Sirimuvva T, Nayan N, Shukla AK, Murty SVSN, Pramod SL, et al. Effect of carbon nanotube dispersion on mechanical properties of aluminum-silicon alloy matrix composites. J Mater Eng Perform. 2014;23:1028–37.
[87] Junaedi H, Abdo HS, Khalil KA, Almajid AA. Aluminum–carbon metal matrix composites: effect of carbon fiber and aspect ratio on the mechanical properties. Adv Mater Res. 2015;1123:119–22.
[88] Bauri R, Yadav D, Suhas G. Effect of friction stir processing (FSP) on microstructure and properties of Al–TiC in situ composite. Mater Sci Eng A. 2011;528:4732–39.